Hybrid additive manufacturing of an electron beam powder bed fused Ti6Al4V by transient liquid phase bonding

Available online at www.sciencedirect.com

jmr&t Journal of Materials Research and Technology

journal homepage: www.elsevier.com/locate/jmrt

Original Article

Hybrid additive manufacturing of an electron beam powder bed fused Ti6Al4V by transient liquid phase bonding

Hamid Reza Ghorbani [a], *Mohammad Hossein Mosallanejad* [a,b], *Masoud Atapour* [a,*], *Manuela Galati* [b], *Abdollah Saboori* [a,b]

[a] *Department of Materials Engineering, Isfahan University of Technology, 84156-83111, Isfahan, Iran*
[b] *Integrated Additive Manufacturing Center, Department of Management and Production Engineering, Politecnico di Torino, Corso Duca Degli Abruzzi 24, 10129 Torino, Italy*

ARTICLE INFO

Article history:
Received 13 June 2022
Accepted 1 July 2022
Available online 13 July 2022

Keywords:
Ti6Al4V
Hybrid additive manufacturing
Electron beam powder bed fusion
Transition liquid phase
Bonding

ABSTRACT

Hybrid Additive Manufacturing (HAM) is a production strategy enhancing the flexibility of the already versatile Additive Manufacturing (AM) techniques. AM of Ti6Al4V, on the other hand, has been of great interest to numerous research works, thanks to the unique corrosion, biomedical and mechanical properties of the alloy. Hence, this research marks the first report on the HAM of Ti6Al4V by Transient Liquid Phase (TLP) bonding of an Electron Beam Powder Bed Fused (EB-PBF) sample to a conventional one. A copper interlayer was used for bonding, and the TLP process was performed at 890 °C and 970 °C for 60 min. Shear strength test was carried out and the results showed the highest shear strengths of 579.3 and 662.5 MPa for TLP bonding at 890 °C and 970 °C, respectively. By increasing the bonding temperature to 970 °C, no Cu-rich phases were observed in the microstructure, as opposed to the 890 °C samples, and a complete isothermal solidification without intermetallic phases was achieved. Moreover, the 970 °C TLP sample was featured with a much better microstructural integrity and homogeneity in both the base metals and the bonded zone. TLP bonding at 970 °C resulted in a more ductile fracture surface than that bonded at 890 °C. The strong differences between the two TLP bonds were primarily attributed to the faster diffusion rate of elements along the joint and base metal at higher temperatures.

1. Introduction

Titanium alloys are used for various applications and industries, such as medical, aerospace, and automotive applications, due to their unique properties, including high specific strength, superior biocompatibility, good mechanical properties, low modulus of elasticity, low density, and good corrosion resistance [1–4]. In fact, titanium alloys are widely regarded as the most attractive metallic materials for

* Corresponding author.
E-mail address: m.atapour@iut.ac.ir (M. Atapour).
https://doi.org/10.1016/j.jmrt.2022.07.009

biomedical applications [5]. Certain applications of Ti alloys require producing complex and near net shape geometries, while titanium and its alloys are difficult to machine due to their costly material loss together with their low thermal conductivity. Also, the poor machinability of titanium and its alloys has limited the use of titanium implants [6,7]. Hence, numerous research works have attempted to combine the benefits of Additive Manufacturing (AM) to benefits of titanium alloys [8–12].

AM is a promising approach used for producing customized and net-shape components with complicated geometry in a layer-wise manner [13]. AM of titanium alloys is challenging the dominance of conventional manufacturing methods and has been used for various industrial applications, especially for the cases where a titanium-based component with a complex geometry is desired [14,15]. Bulk, lattice, and micro-lattice structures of Ti6Al4V alloy have been manufactured using various AM methods such as Laser Powder Bed Fusion (L-PBF) [16–19] and Electron Beam Powder Bed Fusion (EB-PBF) also known as Electron Beam Melting (EBM) [20–23]. It is worth noting that L-PBF and EBM are widely used for producing hard tissue replacements such as AM metal-ceramic and metal implants [4,11]. However, the feedstock materials usually melt at relatively low temperatures in laser-based methods, which can cause residual stresses making the components prone to failure in service. While, in EBM methods, a higher amount of energy is exerted on a preheated substrate [24], which offers the advantage of lowering residual stresses [25]. Consequently, EBM is widely employed for manufacturing Ti-based alloy products, including implants and lattice structures, with the Ti6Al4V alloy being among the most promising Ti alloys for processing via this method [26,27].

Hybrid Additive Manufacturing (HAM) refers to the controlled application of conventional process mechanisms on AM components or the controlled application of AM on products that have been previously subjected to traditional manufacturing processes [28,29]. Besides the size limitations often encountered during the AM routes, in some cases, it is not economical or technically possible to make the whole product by AM. Under the circumstances, AM parts may be required to be joined to conventionally manufactured products, sometimes with the same chemical compositions. Also, the bonding of AM–conventionally manufactured products can be a useful and cost-effective approach to repair of damaged parts. Among the joining techniques, diffusion bonding methods such as transient liquid phase bonding (TLP) can keep the AM rapidly solidified microstructure intact by applying lower amounts of energy to the counterparts, as opposed to fusion welding methods where the energy input is significant.

Published research works on the TLP bonding of Ti-based alloys are divided into similar [30–32] and dissimilar TLP bonding. The latter constitute bonding with alloys such as Ti_2AlNb alloy [33], Al-based alloys [34–39], Mg-based alloys [1,40–46], Co–Cr–Mo alloys [3,47], various steels [48–53], and composites [54,55]. Generally, increasing the time or temperature of the TLP bonding process significantly facilitates the occurrence of isothermal solidification, which in turn avoids the formation of intermetallic phases, improves

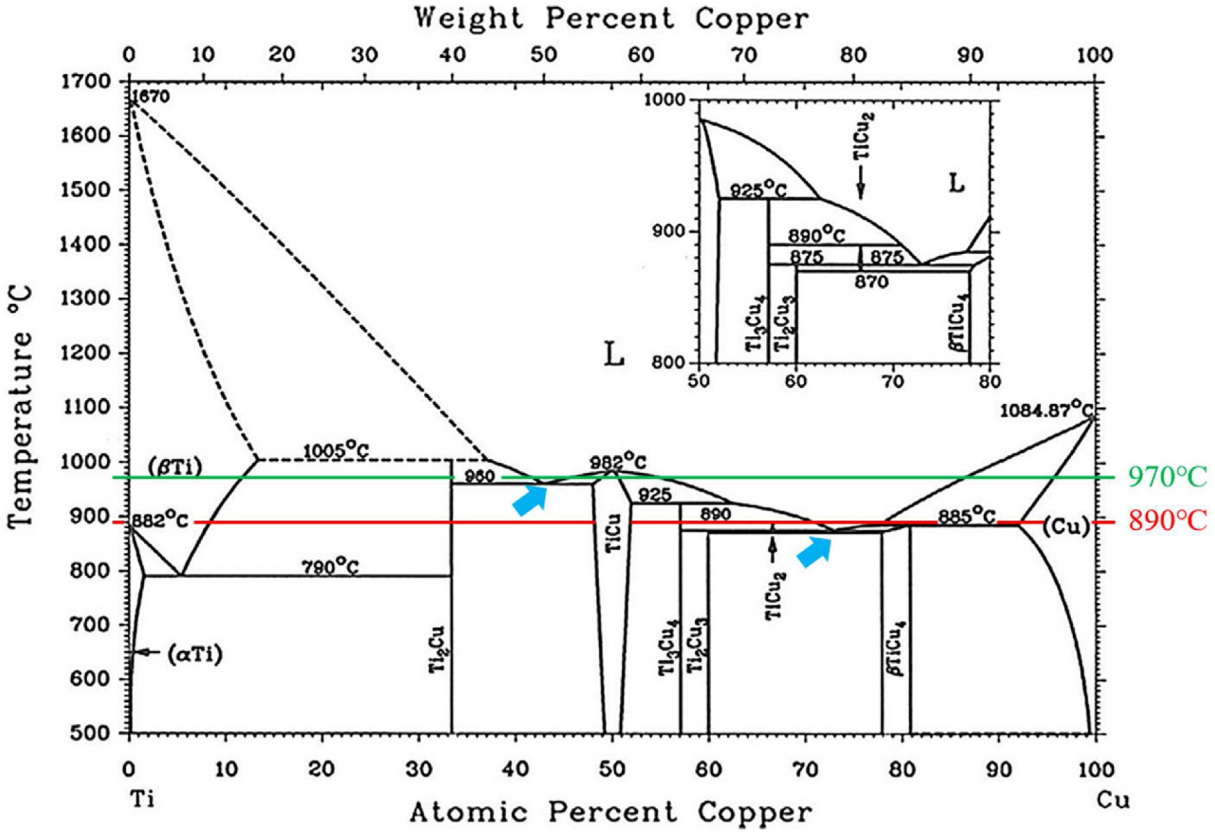

Fig. 1 – Ti–Cu phase diagram.

Table 1 – Chemical composition of the base Ti64 alloys.

	Ti	Al	V	Cu	Mg	Si	Fe	Cr	Sn	C	O	N	H
Conventional	Bal.	5.34	3.84	<1.0	–	–	<0.1	<0.02	<0.50				
Arcam powder	Bal.	6.41	3.86	–			0.19			0.02	0.09	0.01	0.002

microstructure uniformity, and enhances bonding and mechanical properties. Moreover, the lower the interlayer thickness, the lower the isothermal solidification time and the higher the shear strength. According to the previous reports, 60 min long TLP is suggested to be long enough for a complete isothermal solidification [3,47–53,56,57].

To the best of the authors' knowledge, there is no published work on similar or dissimilar TLP bonding of AM alloys to additively or conventionally manufactured alloys. Hence, this work reports the first investigation on dissimilar TLP bonding of AM and conventional Ti6Al4V alloy with Cu foil interlayer. Considering that the two eutectic temperatures observed in the Ti–Cu phase diagram (~875 °C and ~960 °C – Fig. 1) have not been compared in TLP processes yet, the current text mainly aims to assess the feasibility of producing Ti6Al4V samples following the HAM approach through the TLP bonding method at temperatures above the mentioned eutectic transformations temperatures. Microstructural and mechanical characterizations were conducted to evaluate the effect of temperature on the formed bonds.

2. Materials and methods

2.1. Materials

Conventional and AM Ti6Al4V samples were used as base metals in the form. They are named EBM-Ti6Al4V and conventional-Ti6Al4V (wrought-Ti6Al4V) alloys, respectively. To produce the EBM cylindrical samples, extra-low interstitials (ELI) grade Arcam Ti–6Al–4V powder was used as the starting material. The Chemical composition of the conventional-Ti6Al4V and Arcam ELI Ti–6Al–4V powder are shown in Table 1. The starting ELI Ti–6Al–4V powder contains reduced levels of carbon, nitrogen, oxygen, and iron. Finally, a 20 μm thick pure Cu foil was employed as the interlayer.

2.2. Additively manufactured samples

The starting powders were 45–106 μm in diameter and approximately 75 μm volume median diameter. EBM Ti–6Al–4V samples were produced based on the standard Arcam A2X build theme for Ti–6Al–4V (60 kV accelerating voltage, 50 μm layer thickness, and software version of 5.2.52) [58,59]. The unmelted powder was blown off in a Powder Recovery System (PRS) employing the same powder and compressed air.

2.3. TLP bonding of the samples

Cylindrical specimens with 5 mm diameter and 5 mm height were cut from the as-built EBM-Ti6Al4V samples, and the same diameter was considered for the conventional-Ti6Al4V alloy. The sample preparation was carried out using an Electrical Discharge Machining (EDM) machine. The joint surface of the samples was ground and polished. The polished samples were ultrasonically washed in acetone along with the Cu foil. The TLP items were then pickled for 3 min in 20% HCl + 80% distilled water solution in order to remove surface oxides. Next, they were degreased once again in an ultrasonic bath with acetone and remained in ethanol until the TLP process started. Finally, the samples and Cu interlayer were mounted in the TLP fixture under a fixed pressure. The TLP bonding process was carried out in a vacuum furnace under a vacuum of 10^{-5} mbar at temperatures of 890 °C and 970 °C for 1 h, followed by furnace cooling to the room temperature. The heating rate was 10 °C/min.

2.4. Characterizations

In order to obtain the microhardness profile of the TLP bonded region, microhardness measurements were carried out under a 50 g load on the etched microstructures. Shear strength tests

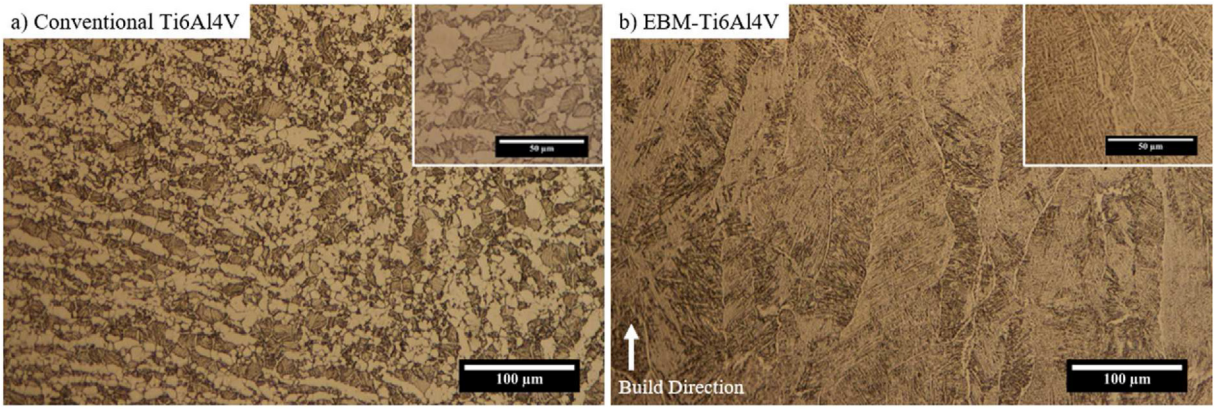

Fig. 2 – Microstructures before the TLP-bonding in a) conventional-Ti6Al4V and b) EBM–Ti6Al4V.

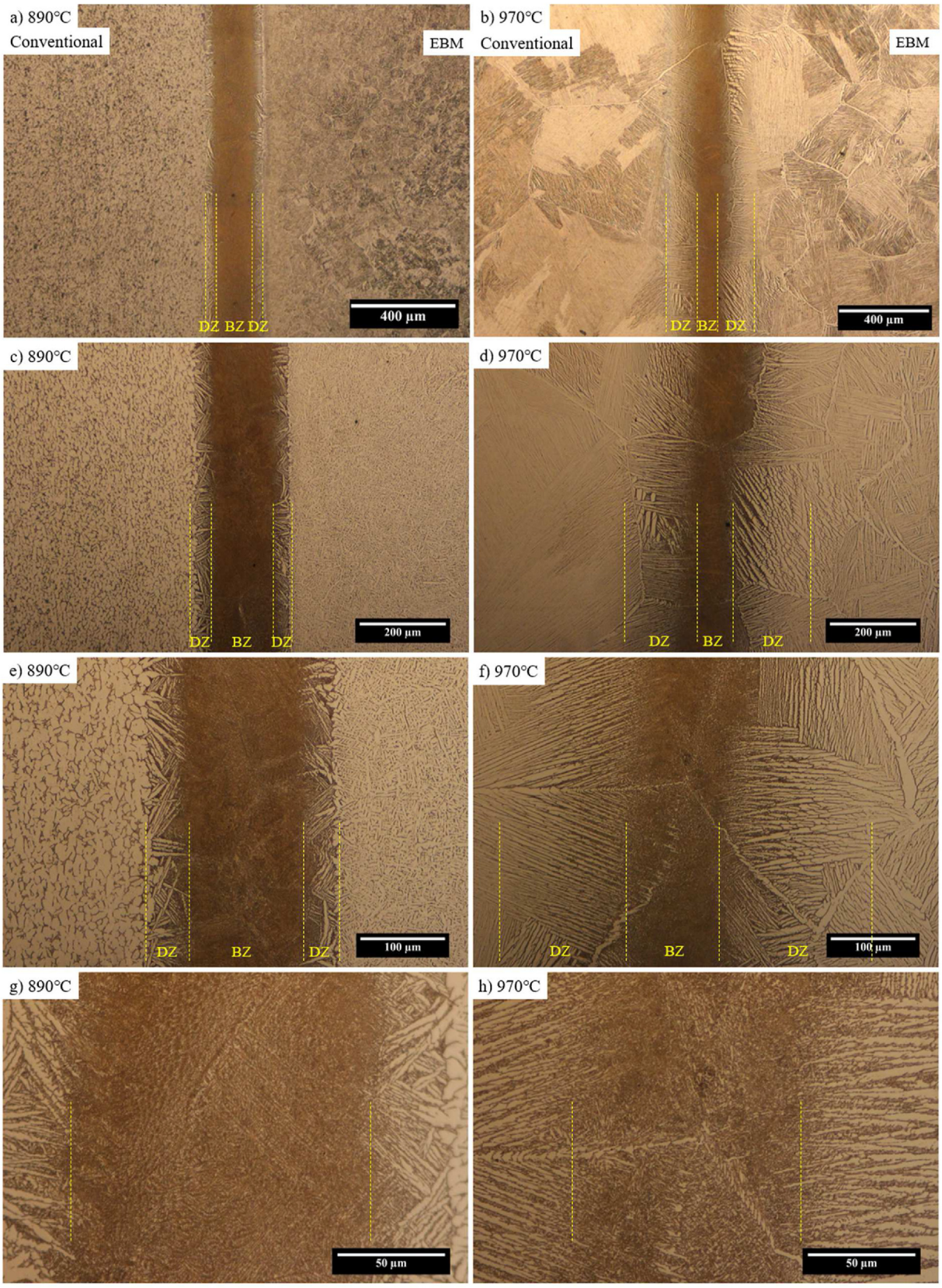

Fig. 3 – OM micrographs of the bonded samples (a, c, e and g) at 890 °C and (b, d, f and h) at 970 °C.

Table 2 – Approximate TLP joint zone width (μm) based on SEM images.

TLP bonding conditions	DZ-conventional side	BZ	DZ-additive side	Joint zone
890 °C/1 h	55	189	51	295
970 °C/1 h	175	131	185	491

(with 1 mm/min crosshead speed) were used to determine the room temperature shear strength of the cylindrical TLP-bonded samples with 5 mm diameter and 10 mm height. Each test was repeated twice. The 600 ml H_2O + 25 ml HNO_3 + 10 ml HF solution was used as the etchant. Microstructures were investigated using Optical Microscopy (OM) (Nikon EpipHot 300) and Scanning Electron Microscopy (SEM) (PhilipsXI30) equipped with Energy Dispersive Spectroscopy (EDS).

3. Results and discussion

3.1. *Microstructural investigations*

The microstructure of the base alloys before the TLP-bonding is shown in Fig. 2. Two light and dark areas are observed in the microstructure of both alloys, which indicate α and β phases, respectively. The microstructure of the conventional—Ti6Al4V alloy consisted of blocks and blades of α phase within the β phase matrix (Fig. 2a). The α phase blades are observable in higher magnification shown in the inset of Fig. 2a. The microstructure of the EBM—Ti6Al4V alloy consisted of prior β columnar grains with ultra-fine α blades within the β phase matrix (Fig. 2b).

Figure 3 shows the microstructures of TLP bonded samples that consisted of three main zones of base metals (BM), diffusion zone (DZ), and bonded zone (BZ). It is worth noting that the diffusion zone (DZ) plus bonded zone (BZ) is named the joint zone (JZ). Figure 3 shows excellent bonding between base metals in both TLP conditions with no observable defect, thanks to the intensive diffusion rate and a highly symmetric joint zone. The diffusion zone is described as the diffusion into the base metals. Table 2 shows the approximate width of the TLP joint zone (DZ + BZ). It can be noted that an increase in the temperature of TLP bonding from 890 °C to 970 °C increased the width of the joint zone, decreased the bonded zone's width and increased the diffusion zone's width (Fig. 3). These features are controlled by the diffusion rate of the elements and the isothermal solidification behavior of the formed liquid. It should be added that increasing the temperature of TLP bonding, enhances the diffusion rate of the elements and isothermal solidification. An obvious sharp interface was observed between the DZ and BM zones at 890 °C sample compared with the diffuse one observed for the 970 °C sample. The interface between the DZ and BM zones of the 970 °C sample is indicative of an intensive diffusion, which results in microstructural changes in the base metal and a better TLP bonding. Alpha phases formed at the grain boundaries of prior equiaxed beta grains are observed as initiating from the diffusion zones of EBM and conventional sides, touching each other at the center of the bonded zone. This feature reveals the occurrence of isothermal solidification. While formation of equiaxed grains was observed in the diffusion zone of both TLP bonding conditions (890 °C and 970 °C), a clearer grain boundary was observed for the 970 °C sample thanks to the higher diffusion rate at a higher temperature.

There was not a significant microstructural change in the conventional and EBM Ti6Al4V side upon TLP bonding at 890 °C, with the blocks and blades of α phase experiencing a negligible growth, and a reduction in the amount of the β phase. It is important to note that the microstructures of the additive Ti6Al4V alloy shown in Fig. 3 are from planes normal to the build direction, which is why the columnar grains are not seen in Fig. 3, as observed in Fig. 2b. TLP bonding at 970 °C, however, induced a significant microstructural change in both the base metals of the conventional and EBM Ti6Al4V. In other words, the microstructure of the conventional Ti6Al4V side was changed from blocks and blades of α phase within β phase matrix to coarse equiaxed beta grains containing α blades. The coarsening of microstructure in the EBM Ti6Al4V side was much higher, while it was much finer than the conventional Ti6Al4V side.

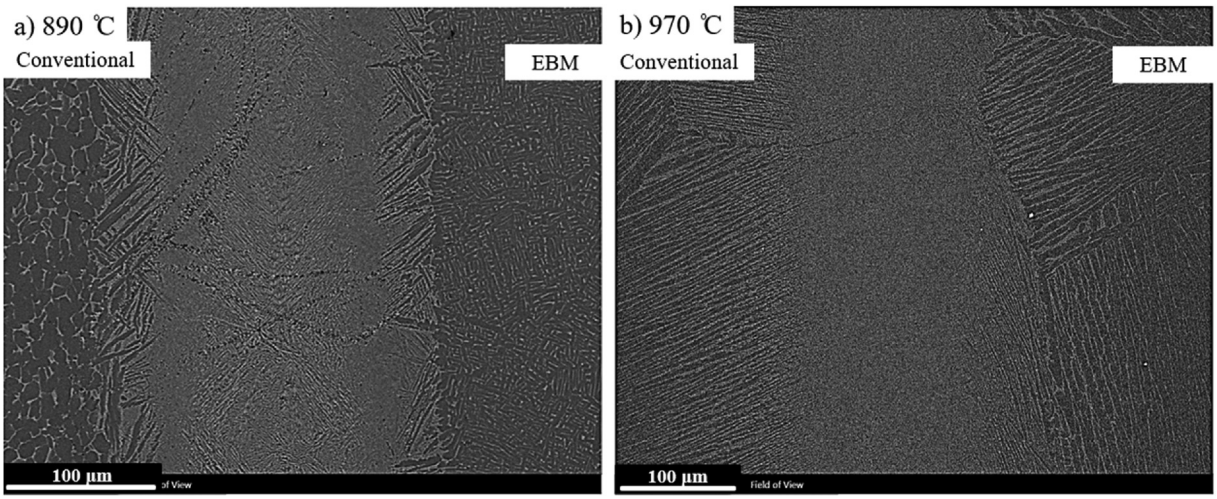

Fig. 4 – BSE Micrographs of the joint zone in the TLP bonded samples, a) 890 °C and b) 970 °C.

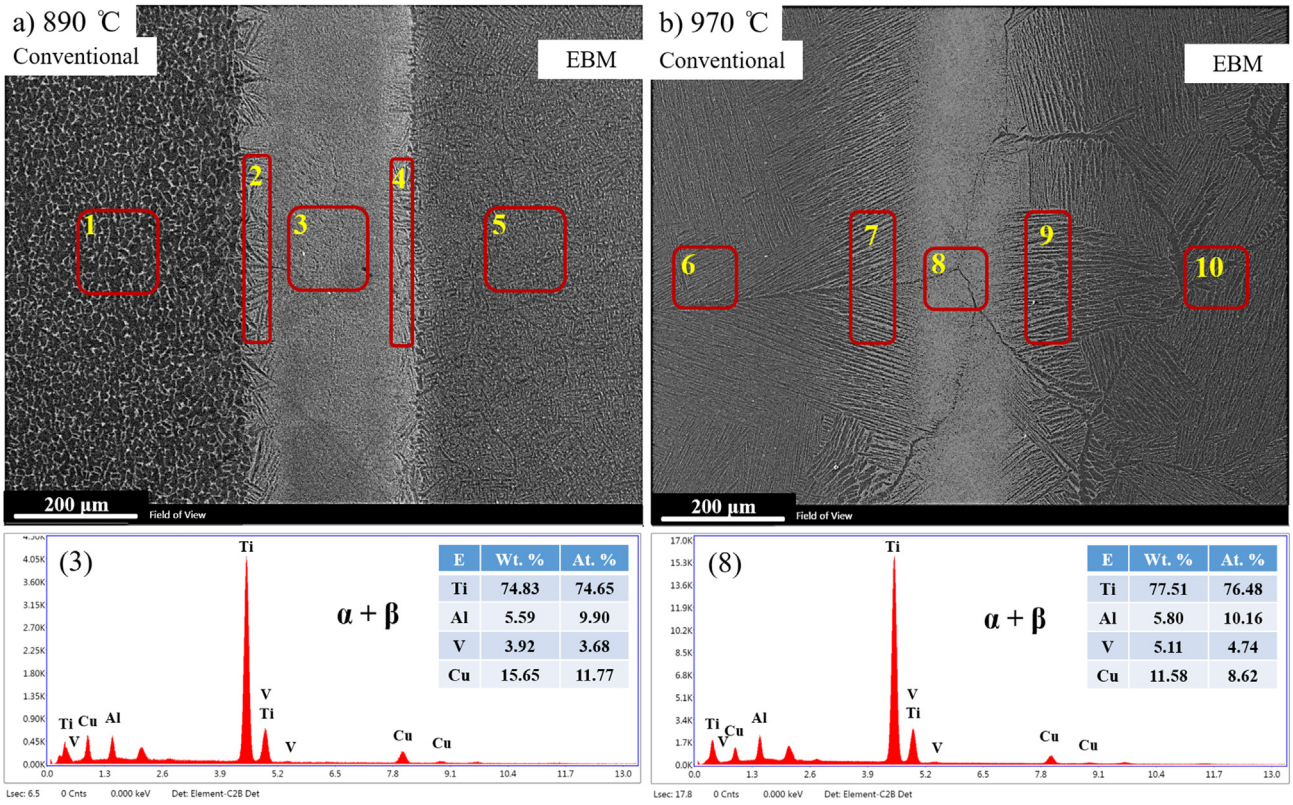

Fig. 5 – SEM micrographs with EDS analysis of different areas in the bonded samples at a) 890 °C and b) 970 °C.

Figure 4 shows the backscattered electron (BSE) micrographs of the joint zone following TLP bonding at 890 °C and 970 °C. The α and β phases are observed with respectively dark gray and light gray colors. A higher amount of β phases is observed in the joint zone for the 890 °C sample. Moreover, a few bright points in Fig. 4a can be Cu-rich zones like Ti_2Cu phases. The microstructure of the bonded zone in Fig. 4b is very uniform, without the formation of intermetallic phases. The SEM micrographs also verified the formation of a diffuse interface for the 970 °C sample, as opposed to the sharp one observed for the 890 °C one.

Figure 5 shows SEM micrographs of the base metals and joint zones in TLP bonded samples and EDS analysis of the BZ (areas 3 and 8). Chemical compositions of the base metals and joint zones are determined by EDS area analysis represented in Table 3. The interlayer was pure Cu foil before the TLP bonding process, but following the TLP bonding process, the Cu content was reduced to 15.6 and 11.6 wt.% in the bonding zone based on the EDS analysis (areas 3 and 8). It reveals the complete dissolution of the Cu interlayer during the TLP process. The Cu content in the joint zone following TLP bonding at 970 °C is lower than TLP bonding at 890 °C. Thus bonding quality at 970 °C is much better and desirable in terms of the microstructural homogeneity. According to Table 3, the Cu content in the DZ for both conventional and EBM sides was similar at 890 °C. However, Cu content on the DZ-EBM side was lower than on the DZ-Conventional side for the sample bonded at 970 °C. It can imply a faster diffusion of Cu at 970 °C in the EBM Ti6Al4V due to its rapidly solidified structure.

Table 3 – Results of Area EDS analysis in Fig. 5 (Wt.%).

EDS	Ti	Al	V	Cu	Area	Suggested phases	Boding temperature
1	88.9	6.6	4.4	0	Conventional Ti6Al4V	Ti (α+β)	890 °C
2	80.8	6.1	4.6	8.5	DZ-Conventional side	Ti (α+β)	
3	74.8	5.6	3.9	15.6	Bonded zone	Ti (α+β)	
4	80.7	6.2	4.9	8.2	DZ-EBM side	Ti (α+β)	
5	88.9	6.6	4.5	0	EBM Ti6Al4V	Ti (α+β)	
6	88.6	6.5	4.8	0	Conventional Ti6Al4V	Ti (α+β)	970 °C
7	80.2	5.9	5.7	8.2	DZ-Conventional side	Ti (α+β)	
8	77.5	5.8	5.1	11.6	Bonded zone	Ti (α+β)	
9	83.8	5.9	4.4	5.9	DZ-EBM side	Ti (α+β)	
10	89.1	5.9	5.0	0	EBM Ti6Al4V	Ti (α+β)	

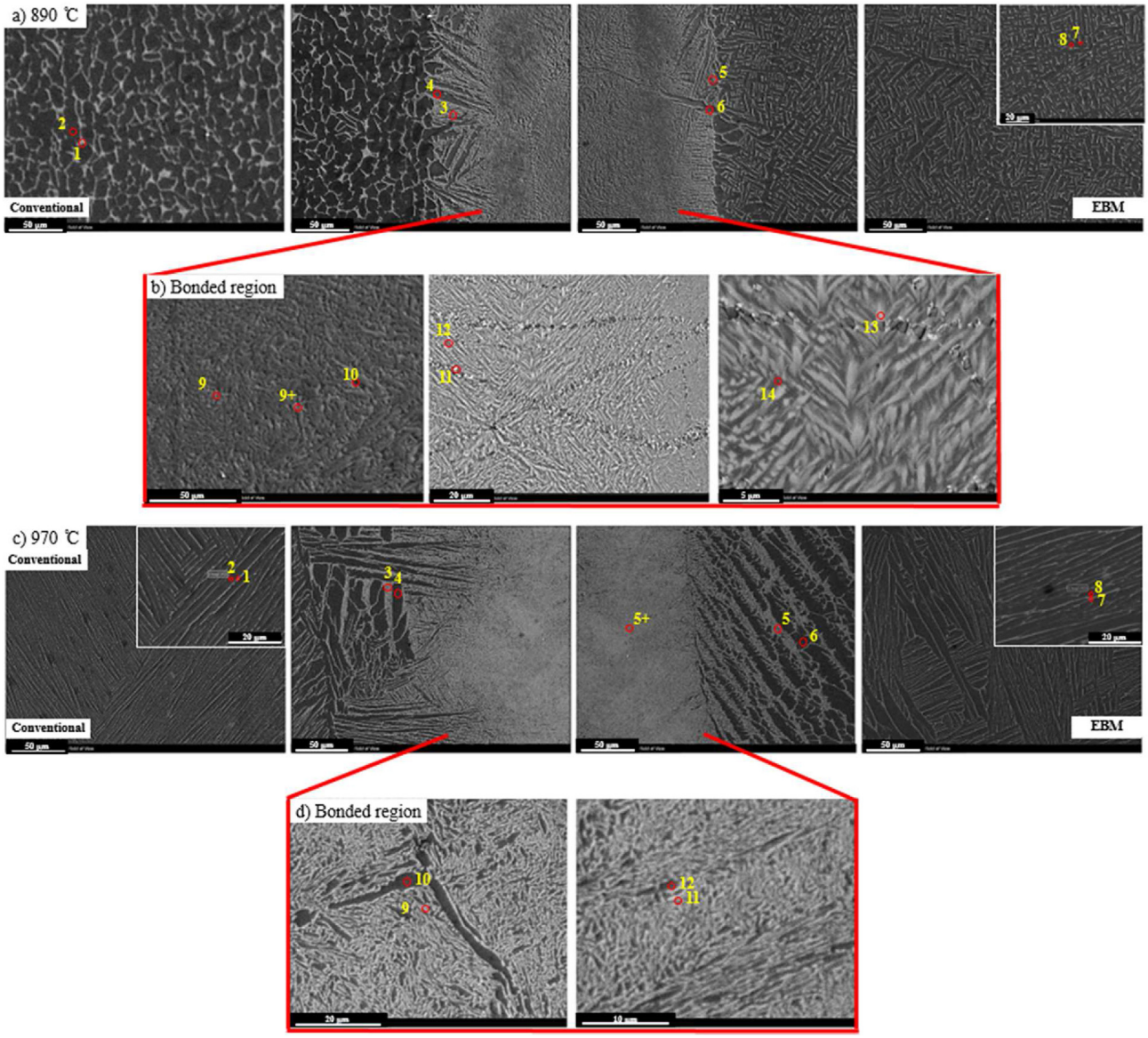

Fig. 6 – SE and BSE micrographs with point EDS analysis of phases in various zones (base metals, diffusion zones, and bonding zone) of the bonded samples at (a and b) 890 °C and (c and d) 970 °C.

Figure 6 shows the SEM micrograph of the TLP bonded samples, focused on the bonded zone. Table 4 presents the results of the EDS point analysis in Fig. 6. The α, β phase, and other possible phases were analyzed in each zone. Both base metals did not have Cu content far from the joint zone. Cu was enriched in β phase more than α phase in both DZ and BZ following TLP bonding at 890 °C and 970 °C. There are some Cu enriched bright phases (up to 29 wt. % Cu) in the bonded zone of the sample bonded at 890 °C (Fig. 6b) that might be Cu enriched phases like Ti_2Cu phases. Interestingly there are no Cu enriched bright phases in the sample bonded at 970 °C. The maximum Cu content is about 11 wt. % and the microstructure of the DZ and BZ are very uniform. Due to higher bonding temperature and faster diffusion rate, all alloying elements from base metals and interlayer (especially Cu) could diffuse in and out of the joint zone. It can be said that, complete isothermal solidification was achieved following TLP bonding at 970 °C. It is worth noting that based on Eq. (1), the diffusion coefficient (D) of elements is a function of temperature, and it will be increased by increasing the temperature. Thus, diffusion of elements at 970 °C is faster and higher than ones at 890 °C. Based on the Fick's second law (Eq. (2)) increase in diffusion coefficient will increase the rate of content change $\frac{\partial C}{\partial t}$ of elements and leads to faster diffusion.

$$D = D_0 \exp\left(\frac{-Q}{RT}\right) \tag{1}$$

$$\frac{\partial C}{\partial t} = \frac{\partial}{\partial x} D \frac{\partial C}{\partial x} \text{ (Fick's second law) [60]} \tag{2}$$

Table 4 – Results of Point EDS analysis in Fig. 6 (Wt.%).

EDS	Ti	Al	V	Cu	Area	Suggested phases	Phase color	Boding temp. (°C)
1	82.08	3.6	14.3	0	Conventional Ti6Al4V	Ti (β)	Light	890°C
2	91.0	7.5	1.5	0		Ti (α)	Dark	
3	79.2	5.7	4.8	10.4	DZ-Conventional side	Ti (β)	Light	
4	88.0	7.3	2.6	2.0		Ti (α)	Dark	
5	79.2	4.7	8.1	8.0	DZ-EBM side	Ti (β)	Light	
6	88.9	7.4	1.7	1.9		Ti (α)	Dark	
7	84.7	5.5	9.8	0	EBM Ti6Al4V	Ti (β)	Light	
8	89.3	7.3	3.4	0		Ti (α)	Dark	
9	73.6	5.7	3.3	17.4	Bonded zone	Ti (β)	Light	
9+	71.4	5.5	3.4	19.7		Ti (β)	Light	
10	74.8	5.4	7.3	12.4		Ti (α)	Dark	
11	71.4	3.6	3.0	22.0		Ti (β) Cu-rich or Ti_2Cu	Bright	
12	77.0	3.6	4.0	15.4		Ti (α)	Dark	
13	64.2	2.6	3.4	29.8		Ti (β) Cu-rich or Ti_2Cu	Light	
14	77.1	3.0	4.5	15.3		Ti (α)	Dark	
1	84.5	4.8	10.7	0	Conventional Ti6Al4V	Ti (β)	Light	970°C
2	89.8	6.9	3.3	0		Ti (α)	Dark	
3	78.7	4.6	5.4	11.3	DZ-Conventional side	Ti (β)	Light	
4	89.45	6.8	1.7	2.0		Ti (α)	Dark	
5+	80.3	5.2	4.1	10.4	Bonded zone	Ti (β)	Light	
5	77.6	4.3	6.6	11.5	DZ-EBM side	Ti (β)	Light	
6	88.6	6.9	2.3	2.2		Ti (α)	Dark	
7	82.7	5.0	12.3	0	EBM Ti6Al4V	Ti (β)	Light	
8	90.1	6.5	3.4	0		Ti (α)	Dark	
9	75.9	5.4	10.0	8.6	Bonded zone	Ti (β)	Light	
10	87.5	6.9	2.1	3.5		Ti (α)	Dark	
11	78.5	5.7	5.8	10.0		Ti (β)	Light	
12	79.7	5.7	3.8	10.5		Ti (α)	Dark	

Equation (3) is used in several works [41–43,49,60–62] for calculating the required time for isothermal solidification during TLP boning. Based on Eq. (3), the higher the diffusion coefficient (D), the lower the isothermal solidification time (t).

$$t = \frac{W_{max}^2}{16K^2D} \quad (3)$$

In Eq. (3), W_{max} is the maximum width of obtained liquid during dissolution and K is a constant. Further details on values and proposed equations for W_{max} and K can be sought in Refs [32,41–43,60–62]. According to the results published in the literature, a total duration of 60 min was considered for the main steps of TLP bonding (including isothermal solidification) both to conduct a precise comparison between the temperatures and to achieve a complete isothermal solidification.

The EDS line scan results across the TLP joint and base metals are shown in Fig. 7. The distribution of elements is uniform at the TLP joint zones (DZ and BZ), following both TLP bonding at 890 °C and 970 °C. Interestingly, the distribution of alloying elements in the sample bonded at 970 °C is much closer to the base metals than in the sample bonded at 890 °C. Also, the Cu content is low and uniform across the analyzed distance, following bonding at 970 °C (Fig. 7b). Figure 8 shows the EDS map analysis of the TLP joint and the neighbor base metals. A highly uniform distribution of alloying elements in the TLP bonded sample at 970 °C is clearly seen in Fig. 8b. However, TLP bonding at both 890 °C and 970 °C resulted in uniform distribution of alloying elements, but uniformity is remarkably higher in the sample bonded at 970 °C by comparing Figs. 8a and b. This finding further suggests a higher quality TLP bonding at 970 °C.

3.2. *Mechanical properties*

The microhardness profile (hardness versus distance) perpendicular to the joint zone is shown in Fig. 9. The curves in Fig. 9 are trendlines, and the standard deviations of the microhardness results are also shown. The hardness of the EBM Ti6Al4V alloy is slightly higher than the conventional Ti6Al4V. According to the Hall-Petch effect, the higher hardness in the EBM sample can be caused due to the finer microstructure and smaller grain size of the EBM Ti6Al4V [47]. The microhardness profile of both TLP bonding at 890 °C and 970 °C is nearly similar to base metals hardness without any sharp change within the joint zone (DZ and BZ). It suggests that no intermetallic phases were formed in both samples, or at least they were negligible. The solution hardening effect of the solved elements can be responsible for slightly higher hardness in some zones, especially the joint zone. The microhardness profile of the sample bonded at 970 °C is more uniform (Fig. 9b) thanks to the enhanced diffusion rates at higher temperatures.

Figure 10 shows the room temperature shear properties of the samples. The shear strengths of the samples bonded at

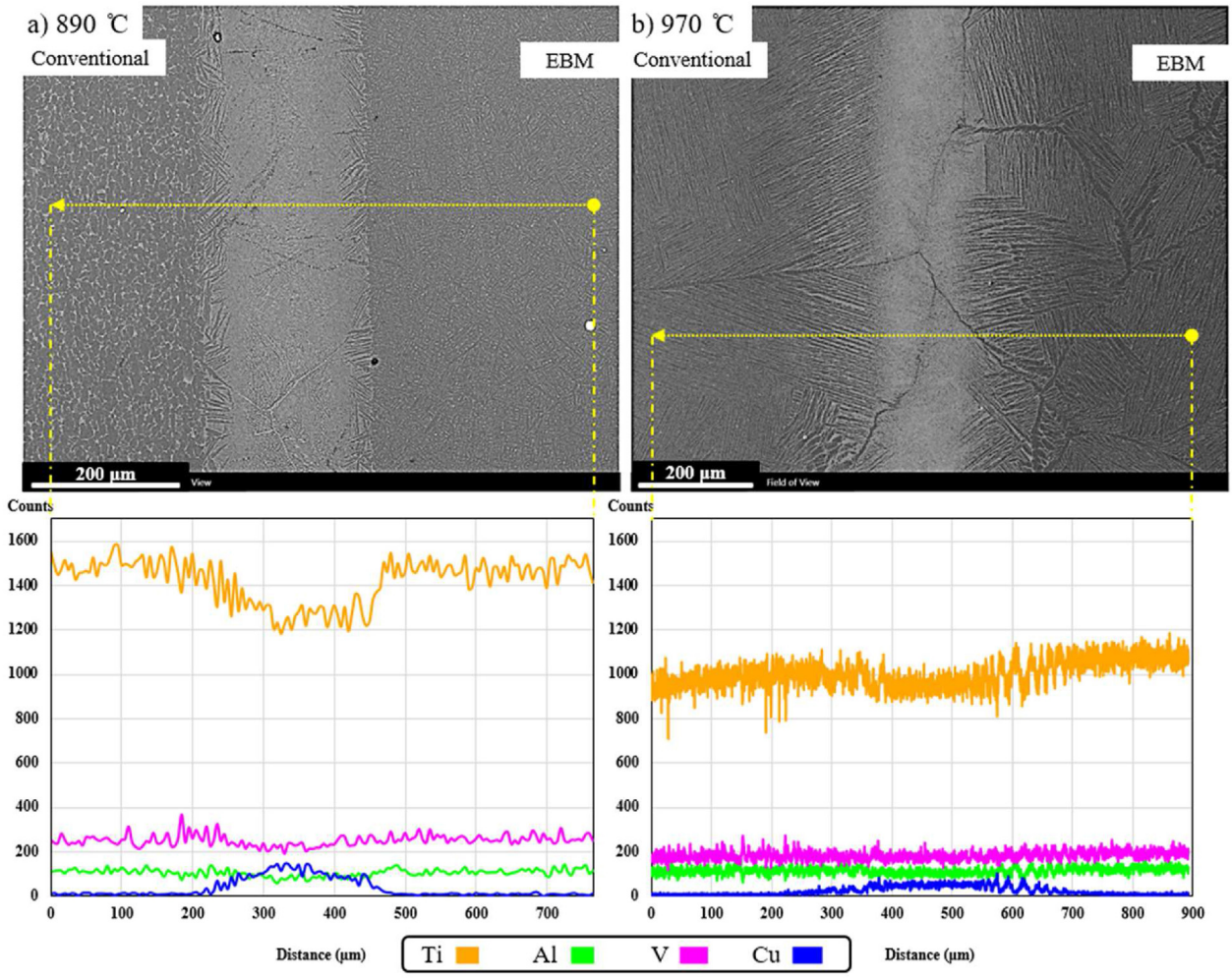

Fig. 7 – SEM Micrographs with line EDS analysis across the bonded zone and neighbor zones in the bonded samples at a) 890 °C and b) 970 °C.

890 °C and 970 °C are 579.3 and 662.5 MPa, respectively. The achieved shear strengths are higher than all of the previous related works (to the best of the authors' knowledge), and the shear strength of the sample bonded at 970 °C is the best one. For example, compared to similar work [31] with 492 MPa shear strength by TLP bonding at 900 °C/300 min and tempering at 520 °C/360 min. Those outstanding mechanical properties are derived from the microstructural properties of the TLP bonded samples. Such as perfect continuous bonding, uniform microstructure of the joint, uniform distribution of elements and composition, mostly isothermal solidification (for sample bonded at 890 °C), fully isothermal solidification (for sample bonded at 970 °C), less intermetallic phase formation (for sample bonded at 890 °C), no intermetallic phase formation (for sample bonded at 970 °C). All of these microstructural features are much better in the sample bonded at 970 °C. These improvements in microstructural features are derived from higher and faster elemental diffusion rate, enough TLP bonding time, and TLP bonding at the higher temperature. The effects of TLP bonding at temperatures slightly above the two eutectic transformations in the Ti–Cu phase diagram, i.e. 890 °C (15 °C above the eutectic transformation at 875 °C) and 970 °C (10 °C above the eutectic transformation at 960 °C), were investigated. Looking at Figs. 9 and 10, it can be concluded that TLP bonding at 970 °C resulted in superior mechanical properties.

Figure 11 shows the SEM micrographs of fractured surfaces following shear strength tests. The results of shear tests suggest semi-ductile or ductile behavior for both TLP bonded samples at 890 °C and 970 °C. The fractured surfaces mainly contained shear flow surfaces (where the material is dragged onto the surface and hereafter is called mashed), dragged (elongated), and normal dimples that are also seen in Refs [63,64]. Numerous mashed and dragged fractured surfaces are observed in Figs. 11a and b; it is worth noting that these (shear flow or mashed surfaces) are not cleavage patterns since cleavage patterns mostly contain flat surfaces or facets that are different from the mashed patterns (flow and drag of material). These mashed surfaces were formed following the dragging and mashing of the dimples and material. This feature is also seen in Fig. 11c and d. It can be said that following the formation of dimples, they were enlarged,

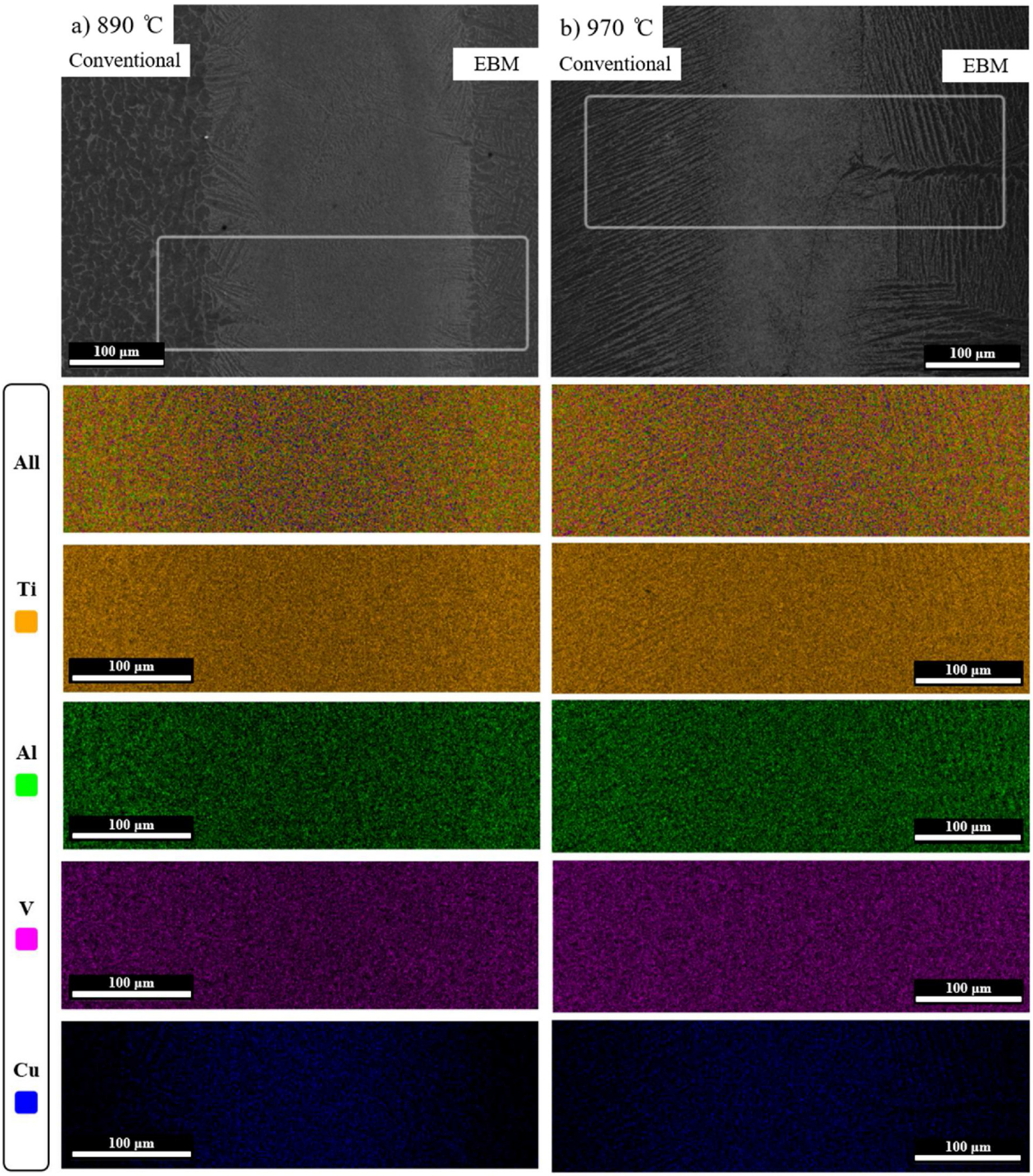

Fig. 8 – SEM Micrographs with Map EDS analysis of the bonded zone and neighbor zones in the bonded samples at a) 890 °C and b) 970 °C.

joined together, and dragged towards the shear force during the shear test. Then, some areas were fractured, and in some other areas, the dragged dimples and material were mashed. It was observed that the fractured counterparts for the sample bonded at 970 °C were elongated towards the tear stress direction, indicating the fracture was ductile, and a significant amount of plastic deformation had occurred before the fracture point. It can also be observed that the fracture surface of the sample bonded at 970 °C is much more ductile than the sample bonded at 890 °C, indicating a more desirable bonding.

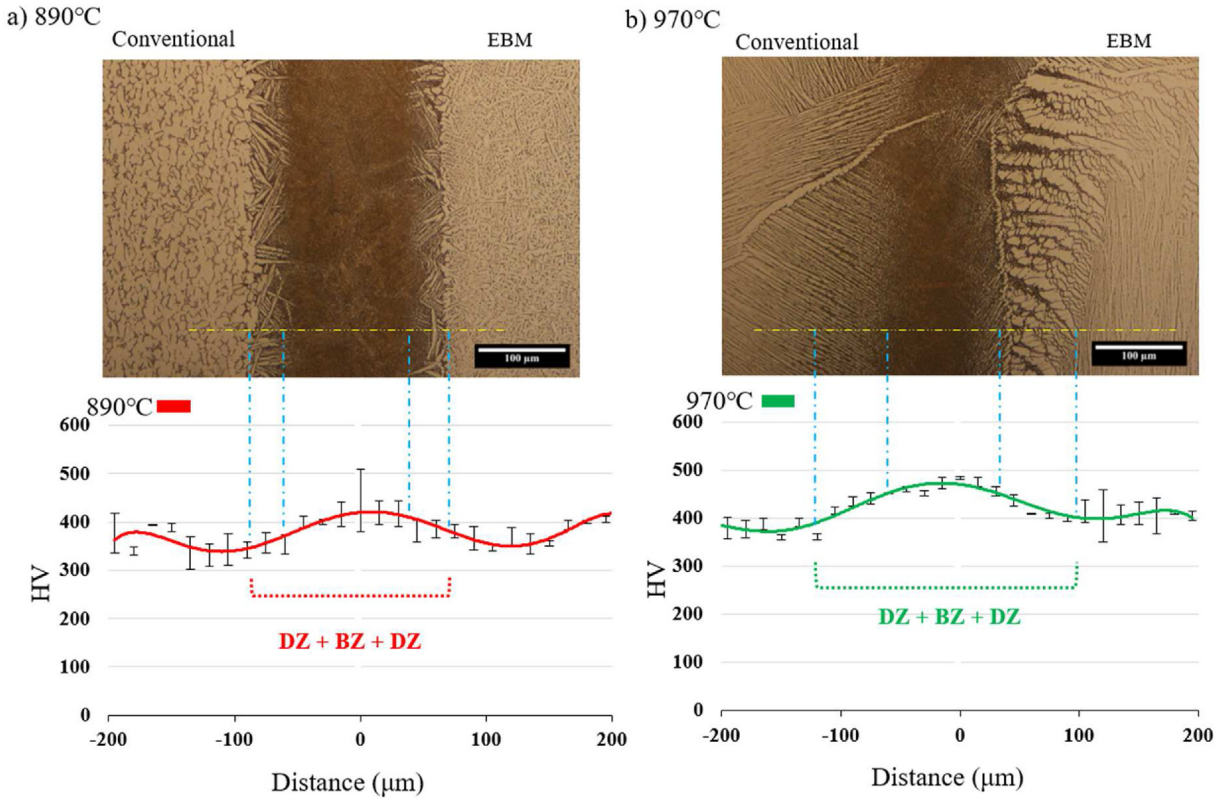

Fig. 9 – Microhardness profile of the bonded zone and neighbor zones in the bonded samples at a) 890 °C and b) 970 °C.

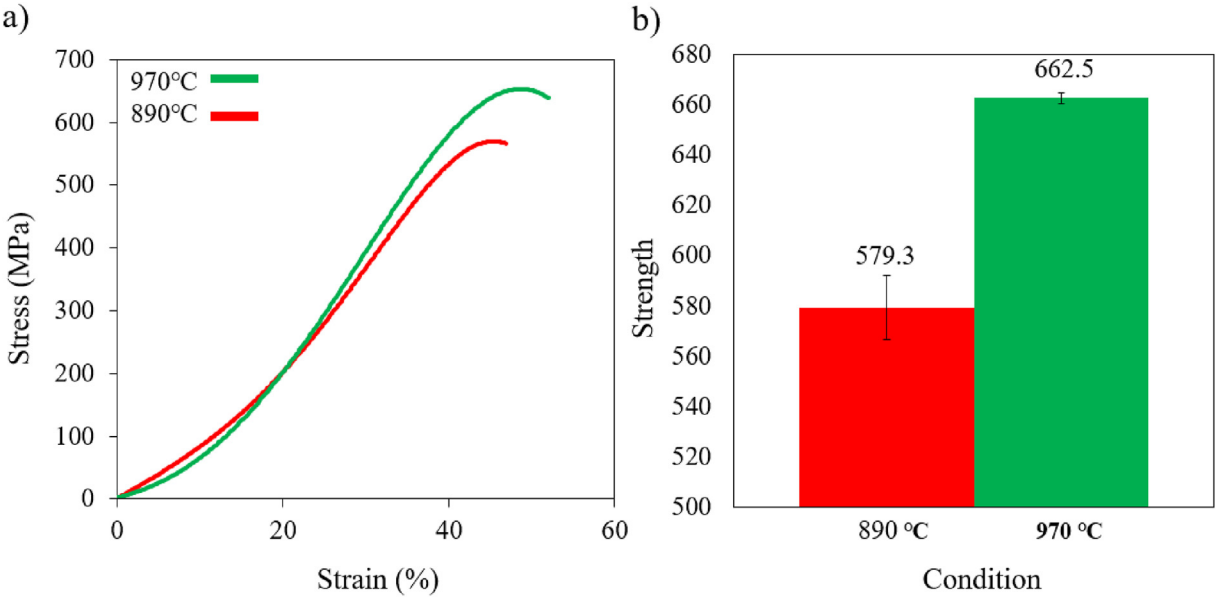

Condition	Strength (MPa)	Strain (%)
890 °C	579.3 ± 12.7	35.9 ± 9
970 °C	662.5 ± 2	42.4 ± 8.4

Fig. 10 – Mechanical properties of the bonded samples a) typical stress–strain curves and b) average shear strengths.

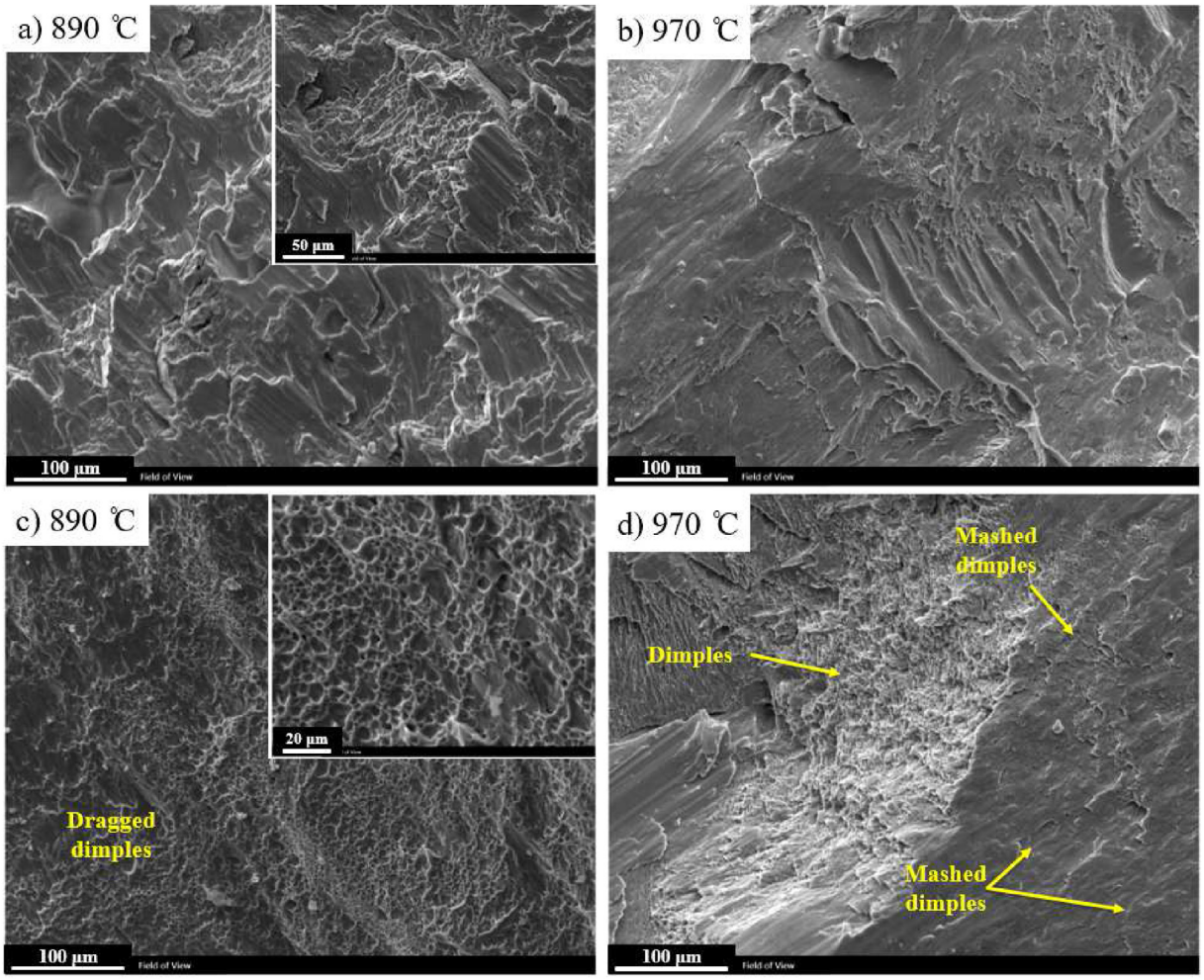

Fig. 11 – Fracture surfaces of the samples bonded at (a and c) 890 °C and (b and d) 970 °C.

4. Conclusions

Hybrid Additive Manufacturing via TLP bonding of an additive manufactured sample to a conventional one was investigated for the first time. This work studied dissimilar TLP bonding between EBM Ti6Al4V and conventional Ti6Al4V alloys using pure Cu foil as an interlayer. Effects of two different Ti–Cu eutectic temperatures on the TLP bonding and its features such as microstructural and mechanical properties were investigated. The main results are as follows:

1) Dissimilar TLP bonding between additively manufactured and conventional Ti6Al4V alloys was successfully achieved for 60 min at both temperatures of 890 °C and 970 °C.
2) Increasing temperature caused an increase in the width of the joint zone due to the increased volume of eutectic melt. The width of the diffusion zone was increased, but the width of the bonded zone was decreased due to more isothermal solidification.
3) Increasing TLP bonding temperature from 890 °C to 970 °C leads to complete isothermal solidification. Also, it leads to much better microstructural integrity and homogeneity in both the base metals and the joint zone.
4) There were some Cu-rich phases (probably β-Cu rich or Ti2Cu) in the microstructure of the sample bonded at 890 °C, which was not observed at 970 °C.
5) Increasing the TLP bonding temperature from 890 °C to 970 °C enhanced the average shear strength from 597.3 MPa to 662.5 MPa. This significant improvement was attributed to the formation of a well-bonded zone thanks to the enhanced diffusion rates at higher temperatures. It was further noticed that the sample bonded at 970 °C had more ductile fracture than the sample bonded at 890 °C.
6) It can be concluded that the recommended joining conditions via TLP method for bonding EBM Ti6Al4V to a conventional one using Cu interlayer is bonding at is 970 °C for 60 min.

CRediT authorship contribution statement

Atapour Masoud: Supervision, Project administration, Validation, Writing – review & editing, Ghorbani Hamid Reza: Writing – review & editing, Investigation. Mohammad Hossein Mosallanejad: Writing – original draft, Methodology, Investigation, Conceptualization. Manuela Galati:

Investigation, validation, EBM sample production; Saboori Abdollah: Conceptualization, EBM sample production, Supervision, Resources, Writing – review & editing.

Declaration of Competing Interest

The authors declare that they have no known competing financial interests or personal relationships that could have appeared to influence the work reported in this paper.

REFERENCES

[1] AlHazaa A, Alhoweml I, Shar MA, Hezam M, Abdo HS, AlBrithen H. Transient liquid phase bonding of Ti-6Al-4V and Mg-AZ31 alloys using Zn coatings. Materials 2019;12. https://doi.org/10.3390/ma12050769.

[2] Saboori A, Gallo D, Biamino S, Fino P, Lombardi M. An overview of additive manufacturing of titanium components by directed energy deposition: microstructure and mechanical properties. Appl Sci 2017;7. https://doi.org/10.3390/app7090883.

[3] Vazirian S, Farzadi A. Dissimilar transient liquid phase bonding of Ti–6Al–4V and Co–Cr–Mo biomaterials using a Cu interlayer: microstructure and mechanical properties. J Alloys Compd 2020;829:154510. https://doi.org/10.1016/j.jallcom.2020.154510.

[4] da Silva LRR, Sales WF, Campos FAR, de Sousa JAG, Davis R, Singh A, et al. A comprehensive review on additive manufacturing of medical devices. Prog Addit Manuf 2021;6:517–53. https://doi.org/10.1007/s40964-021-00188-0.

[5] Elias CN, Lima JHC, Valiev R, Meyers MA. Biomedical applications of titanium and its alloys. JOM 2008;60:46–9. https://doi.org/10.1007/s11837-008-0031-1.

[6] Karlsson J, Snis A, Engqvist H, Lausmaa J. Characterization and comparison of materials produced by Electron Beam Melting (EBM) of two different Ti–6Al–4V powder fractions. J Mater Process Technol 2013;213:2109–18.

[7] Galati M, Defanti S, Saboori A, Rizza G, Tognoli E, Vincenzi N, et al. An investigation on the processing conditions of Ti-6Al-2Sn-4Zr-2Mo by electron beam powder bed fusion: microstructure, defect distribution, mechanical properties and dimensional accuracy. Addit Manuf 2022;50:102564. https://doi.org/10.1016/j.addma.2021.102564.

[8] Qian M, Bourell DL. Additive manufacturing of titanium alloys. JOM 2017;69:2677–8. https://doi.org/10.1007/s11837-017-2630-1.

[9] DebRoy T, Wei HL, Zuback JS, Mukherjee T, Elmer JW, Milewski JO, et al. Additive manufacturing of metallic components – process, structure and properties. Prog Mater Sci 2018;92:112–224. https://doi.org/10.1016/j.pmatsci.2017.10.001.

[10] Zhang J, Zhou W, Wang H, Lin K, Chen F. 3D-printed surface promoting osteogenic differentiation and angiogenetic factor expression of BMSCs on Ti6Al4V implants and early osseointegration in vivo. J Mater Sci Technol 2019;35:336–43. https://doi.org/10.1016/j.jmst.2018.09.063.

[11] Liu Y, Li S, Hou W, Wang S, Hao Y, Yang R, et al. Electron beam melted beta-type Ti–24Nb–4Zr–8Sn porous structures with high strength-to-modulus ratio. J Mater Sci Technol 2016;32:505–8. https://doi.org/10.1016/j.jmst.2016.03.020.

[12] Mosallanejad MH, Niroumand B, Aversa A, Manfredi D, Saboori A. Laser powder bed fusion in-situ alloying of Ti-5% Cu alloy: process-structure relationships. J Alloys Compd 2021;857:157558. https://doi.org/10.1016/j.jallcom.2020.157558.

[13] Dadkhah M, Mosallanejad MH, Iuliano L, Saboori A. A comprehensive overview on the latest progress in the additive manufacturing of metal matrix composites: potential, challenges, and feasible solutions. Acta Metall Sin (English Lett) 2021;34:1173–200. https://doi.org/10.1007/s40195-021-01249-7.

[14] Zhang D, Qiu D, Gibson MA, Zheng Y, Fraser HL, StJohn DH, et al. Additive manufacturing of ultrafine-grained high-strength titanium alloys. Nature 2019;576:91–5. https://doi.org/10.1038/s41586-019-1783-1.

[15] Mosallanejad MH, Niroumand B, Aversa A, Saboori A. In-situ alloying in laser-based additive manufacturing processes: a critical review. J Alloys Compd 2021;872:159567. https://doi.org/10.1016/j.jallcom.2021.159567.

[16] Liu L, Chen C, Zhao R, Wang X, Tao H, Shuai S, et al. In-situ nitrogen strengthening of selective laser melted Ti6Al4V with superior mechanical performance. Addit Manuf 2021;46:102142. https://doi.org/10.1016/j.addma.2021.102142.

[17] Keaveney S, Shmeliov A, Nicolosi V, Dowling DP. Investigation of process by-products during the selective laser melting of Ti6AL4V powder. Addit Manuf 2020;36:101514. https://doi.org/10.1016/j.addma.2020.101514.

[18] Achee T, Guss G, Elwany A, Matthews M. Laser pre-sintering for denudation reduction in the laser powder bed fusion additive manufacturing of Ti-6Al-4V alloy. Addit Manuf 2021;42:101985. https://doi.org/10.1016/j.addma.2021.101985.

[19] Hossain U, Ghouse S, Nai K, Jeffers JRT. Mechanical and morphological properties of additively manufactured SS316L and Ti6Al4V micro-struts as a function of build angle. Addit Manuf 2021;46:102050. https://doi.org/10.1016/j.addma.2021.102050.

[20] Del Guercio G, Galati M, Saboori A, Fino P, Iuliano L. Microstructure and mechanical performance of Ti–6Al–4V lattice structures manufactured via electron beam melting (EBM): a review. Acta Metall Sin (English Lett 2020;33:183–203. https://doi.org/10.1007/s40195-020-00998-1.

[21] Montelione A, Ghods S, Schur R, Wisdom C, Arola D, Ramulu M. Powder reuse in electron beam melting additive manufacturing of Ti6Al4V: particle microstructure, oxygen content and mechanical properties. Addit Manuf 2020;35:101216. https://doi.org/10.1016/j.addma.2020.101216.

[22] Del Guercio G, Galati M, Saboori A. Innovative approach to evaluate the mechanical performance of Ti–6Al–4V lattice structures produced by electron beam melting process. Met Mater Int 2021;27:55–67. https://doi.org/10.1007/s12540-020-00745-2.

[23] He X, Li Y, Bi Y, Liu X, Zhou B, Zhang S, et al. Finite element analysis of temperature and residual stress profiles of porous cubic Ti-6Al-4V titanium alloy by electron beam melting. J Mater Sci Technol 2020;44:191–200. https://doi.org/10.1016/j.jmst.2020.01.033.

[24] Mosallanejad MH, Niroumand B, Ghibaudo C, Biamino S, Salmi A, Fino P, et al. In-situ alloying of a fine grained fully equiaxed Ti-based alloy via Electron Beam Powder Bed Fusion Additive Manufacturing process. Addit Manuf 2022;56:102878. https://doi.org/10.1016/j.addma.2022.102878.

[25] Tamayo JA, Riascos M, Vargas CA, Baena LM. Additive manufacturing of Ti6Al4V alloy via electron beam melting for the development of implants for the biomedical industry. Heliyon 2021;7:e06892. https://doi.org/10.1016/j.heliyon.2021.e06892.

[26] Del Guercio G, Galati M, Saboori A. Electron beam melting of Ti-6Al-4V lattice structures: correlation between post heat treatment and mechanical properties. Int J Adv Manuf Technol 2021;116:3535–47. https://doi.org/10.1007/s00170-021-07619-w.

[27] Aversa A, Saboori A, Marchese G, Iuliano L, Lombardi M, Fino P. Recent progress in beam-based metal additive manufacturing from a materials perspective: a review of patents. J Mater Eng Perform 2021;30:8689–99. https://doi.org/10.1007/s11665-021-06273-3.
[28] Pragana JPM, Sampaio RFV, Bragança IMF, Silva CMA, Martins PAF. Hybrid metal additive manufacturing: a state–of–the-art review. Adv Ind Manuf Eng 2021;2:100032. https://doi.org/10.1016/j.aime.2021.100032.
[29] Souflas T, Bikas H, Ghassempouri M, Salmi A, Atzeni E, Saboori A, et al. A comparative study of dry and cryogenic milling for Directed Energy Deposited IN718 components: effect on process and part quality. Int J Adv Manuf Technol 2022;119:745–58. https://doi.org/10.1007/s00170-021-08313-7.
[30] Deng Y, Sheng G, Wang F, Yuan X, An Q. Microstructure evolution and mechanical properties of transient liquid phase bonded Ti–6Al–4V joint with copper interlayer. Mater Des 2016;92:1–7. https://doi.org/10.1016/j.matdes.2015.11.103.
[31] Davoodi Jamaloei A, Salimijazi HR, Edris H, Mostaghimi J. Study of TLP bonding of Ti-6Al-4V alloy produced by vacuum plasma spray forming and forging. Mater Des 2017;121:355–66. https://doi.org/10.1016/j.matdes.2017.02.046.
[32] Tadgell CA, Corbin SF. Determining the mechanisms of dissolution and isothermal solidification kinetics during transient liquid phase bonding of commercially pure titanium using a pure copper interlayer. Mater Today Commun 2020;24:101363. https://doi.org/10.1016/j.mtcomm.2020.101363.
[33] Feng G, Wei Y, Hu B, Wang Y, Deng D, Yang X. Vacuum diffusion bonding of Ti2AlNb alloy and TC4 alloy. Trans Nonferrous Met Soc China 2021;31:2677–86. https://doi.org/10.1016/S1003-6326(21)65684-4.
[34] Anbarzadeh A, Sabet H, Abbasi M. Effects of successive-stage Transient Liquid Phase (S-TLP) on microstructure and mechanical properties of Al2024 to Ti-6Al-4V joint. Mater Lett 2016;178:280–3. https://doi.org/10.1016/j.matlet.2016.04.071.
[35] Naeimian H, Mofid MA. TLP bonding of Ti–6Al–4V to Al 2024 using thermal spray Babbitt alloy interlayer. Trans Nonferrous Met Soc China 2020;30:1267–76. https://doi.org/10.1016/S1003-6326(20)65294-3.
[36] AlHazaa A, Khan TI, Haq I. Transient liquid phase (TLP) bonding of Al7075 to Ti-6Al-4V alloy. Mater Char 2010;61:312–7. https://doi.org/10.1016/j.matchar.2009.12.014.
[37] Kenevisi MS, Mousavi Khoie SM. A study on the effect of bonding time on the properties of Al7075 to Ti–6Al–4V diffusion bonded joint. Mater Lett 2012;76:144–6. https://doi.org/10.1016/j.matlet.2012.02.104.
[38] Kenevisi MS, Mousavi Khoie SM. An investigation on microstructure and mechanical properties of Al7075 to Ti-6Al-4V Transient Liquid Phase (TLP) bonded joint. Mater Des 2012;38:19–25. https://doi.org/10.1016/j.matdes.2012.01.046.
[39] Samavatian M, Khodabandeh A, Halvaee A, Amadeh AA. Transient liquid phase bonding of Al 2024 to Ti–6Al–4V alloy using Cu–Zn interlayer. Trans Nonferrous Met Soc China 2015;25:770–5. https://doi.org/10.1016/S1003-6326(15)63662-7.
[40] AlHazaa AN. Effect of bonding temperature on the microstructure and strength of the joint between magnesium AZ31 and Ti-6Al-4V alloys using copper coatings and tin interlayers. Key Eng Mater 2017;735:34–41. https://doi.org/10.4028/www.scientific.net/KEM.735.34.
[41] Atieh AM, Khan TI. TLP bonding of Ti-6Al-4V and Mg-AZ31 alloys using pure Ni electro-deposited coats. J Mater Process Technol 2014;214:3158–68. https://doi.org/10.1016/j.jmatprotec.2014.07.028.
[42] Atieh AM, Khan TI. Effect of interlayer thickness on joint formation between Ti-6Al-4V and Mg-AZ31 alloys. J Mater Eng Perform 2014;23:4042–54. https://doi.org/10.1007/s11665-014-1179-1.
[43] Atieh AM, Khan TI. Application of Ni and Cu nanoparticles in transient liquid phase (TLP) bonding of Ti-6Al-4V and Mg-AZ31 alloys. J Mater Sci 2014;49:7648–58. https://doi.org/10.1007/s10853-014-8473-z.
[44] Atieh AM, Khan TI. Effect of process parameters on semi-solid TLP bonding of Ti–6Al–4V to Mg–AZ31. J Mater Sci 2013;48:6737–45. https://doi.org/10.1007/s10853-013-7475-6.
[45] Atieh AM, Khan TI. Transient liquid phase (TLP) brazing of Mg-AZ31 and Ti-6Al-4V using Ni and Cu sandwich foils. Sci Technol Weld Join 2014;19:333–42. https://doi.org/10.1179/1362171814Y.0000000196.
[46] Atieh AM, Khan TI. Effect of interlayer configurations on joint formation in TLP bonding of Ti-6Al-4V to Mg-AZ31. IOP Conf Ser Mater Sci Eng 2014;60:12036. https://doi.org/10.1088/1757-899x/60/1/012036.
[47] Vazirian S, Farzadi A. Effect of bonding temperature on microstructure and mechanical properties of dissimilar joint between Ti–6Al–4V and Co–Cr–Mo biomaterials. Mater Sci Eng A 2020;792:139825. https://doi.org/10.1016/j.msea.2020.139825.
[48] Jalali A, Atapour M, Shamanian M, Vahman M. Transient liquid phase (TLP) bonding of Ti-6Al-4V/UNS 32750 super duplex stainless steel. J Manuf Process 2018;33:194–202. https://doi.org/10.1016/j.jmapro.2018.05.014.
[49] Norouzi E, Atapour M, Shamanian M, Allafchian A. Effect of bonding temperature on the microstructure and mechanical properties of Ti-6Al-4V to AISI 304 transient liquid phase bonded joint, vol. 99. Elsevier B.V.; 2016. https://doi.org/10.1016/j.matdes.2016.03.101.
[50] Norouzi E, Atapour M, Shamanian M. Effect of bonding time on the joint properties of transient liquid phase bonding between Ti–6Al–4V and AISI 304. J Alloys Compd 2017;701:335–41. https://doi.org/10.1016/j.jallcom.2017.01.091.
[51] Zakipour S, Halvaee A, Amadeh AA, Samavatian M, Khodabandeh A. An investigation on microstructure evolution and mechanical properties during transient liquid phase bonding of stainless steel 316L to Ti-6Al-4V. J Alloys Compd 2015;626:269–76. https://doi.org/10.1016/j.jallcom.2014.11.160.
[52] Cooke KO, Richardson A, Khan TI, Shar MA. High-temperature diffusion bonding of Ti–6Al–4V and super-duplex stainless steel using a Cu interlayer embedded with alumina nanoparticles. J Manuf Mater Process 2020;4. https://doi.org/10.3390/jmmp4010003.
[53] Elrefaey A, Tillmann W. Evaluation of transient liquid phase bonding between titanium and steel. Adv Eng Mater 2009;11:556–60. https://doi.org/10.1002/adem.200900021.
[54] Liu K, Li Y, Xia C, Wang J. Microstructural evolution and properties of TLP diffusion bonding super-Ni/NiCr laminated composite to Ti-6Al-4V alloy with Cu interlayer. Mater Des 2017;135:184–96. https://doi.org/10.1016/j.matdes.2017.09.028.
[55] Fan D, Li C, Huang J, Yang J, Cui B, Wang W. A novel composite-diffusion brazing process based on transient liquid phase bonding of a Cf/SiC composite to Ti-6Al-4V. Ceram Int 2017;43:13009–12. https://doi.org/10.1016/j.ceramint.2017.06.044.
[56] Karimi MA, Shamanian M, Enayati MH. Microstructural and mechanical properties assessment of transient liquid phase bonding of CoCuFeMnNi high entropy alloy. Trans Nonferrous Met Soc China 2021;31:3063–74. https://doi.org/10.1016/S1003-6326(21)65715-1.

[57] Ajabshiri M, Shamanian M, Ashrafi A, Karimi MA. The effect of bonding time on dissimilar joint properties between inconel 625 and AISI 316L using transient liquid phase bonding method with Cu interlayer. J Mater Eng Perform 2022;31:3311–25. https://doi.org/10.1007/s11665-021-06411-x.
[58] Chen LY, Huang JC, Lin CH, Pan CT, Chen SY, Yang TL, et al. Anisotropic response of Ti-6Al-4V alloy fabricated by 3D printing selective laser melting. Mater Sci Eng A 2017;682:389–95.
[59] Saboori A, Abdi A, Fatemi SA, Marchese G, Biamino S, Mirzadeh H. Hot deformation behavior and flow stress modeling of Ti–6Al–4V alloy produced via electron beam melting additive manufacturing technology in single β-phase field. Mater Sci Eng A 2020;792:139822. https://doi.org/10.1016/j.msea.2020.139822.
[60] Cooke KO, Atieh AM. Current trends in dissimilar diffusion bonding of titanium alloys to stainless steels, aluminium and magnesium. J Manuf Mater Process 2020;4. https://doi.org/10.3390/jmmp4020039.
[61] Zhou Y. Analytical modeling of isothermal solidification during transient liquid phase (TLP) bonding. J Mater Sci Lett 2001;20:841–4. https://doi.org/10.1023/A:1010914813875.
[62] Sawatzky T. Joining of powder metallurgy beta gamma titanium aluminide through diffusion brazing. Carleton University; 2017. https://doi.org/10.22215/etd/2017-11756.
[63] Denti L. Additive manufactured A357.0 samples using the laser powder bed fusion technique: shear and tensile performance. Met 2018;8. https://doi.org/10.3390/met8090670.
[64] Valoppi B, Zhang Z, Deng M, Ghiotti A, Bruschi S, Ehmann KF, et al. On the fracture characterization in double-sided incremental forming of Ti6Al4V sheets at elevated temperatures. Proc Manuf 2017;10:407–16. https://doi.org/10.1016/j.promfg.2017.07.014.